The thermo-therapeutic applications of Chitosan- CTAB coated Nickel Ferrite ($NiFe_2O_4$) magnetic nanoparticles

Hayder Al-Bairmani[1,2], Mahmood Rezaee Roknabadi[1,2*], Mohammad Behdani[1] and Mojtaba Mohammadi[1]

[1]Department of Physics, Faculty of Science, Ferdowsi University of Mashhad, Mashhad, Iran.
[2]Angstrom Thin Film Research Laboratory, Faculty of Science, Ferdowsi University of Mashhad, Mashhad, Iran.

*Corresponding author. E-mail: Roknabad@um.ac.ir;

Abstract

In this study, we used a hydrothermal-assisted co-precipitation method to synthesize the nickel ferrite (FN), Chitosan coated nickel ferrite (FN-Ch) and cetyltrimethylammonium bromide coated nickel ferrite (FN-CT) nanoparticles with small sizes and good biocompatibility. These nanoparticles were then evaluated for their potential use in magnetic hyperthermia. The particles were characterized using a variety of techniques, including X-ray diffraction, transmission electron microscopy (TEM), Fourier transform infrared (FT-IR) spectroscopy, Thermogravimetric Analysis (TGA), Inductively coupled plasma (ICP), magnetic characterization (VSM), zeta potential analysis, and in vivo studies (blood hemolysis and MTT test). The results of the X-ray diffraction analysis showed that the nanoparticles had a spinel phase of $NiFe_2O_4$. TEM analysis revealed that all three samples contained particles with nearly quadrilateral and hexagonal shapes. FT-IR spectroscopy confirmed the presence of Chitosan and CTAB coatings on the particle surface. Magnetic hysteresis curves showed that all of the synthesized samples exhibited superparamagnetic behavior at room temperature. The findings from the ICP analysis indicated that the FN-Ch and FN-CT nanoparticles contained iron and nickel, while no substantial quantities of other trace elements were identified in either of the samples. Blood hemolysis and MTT tests were used to assess the toxicity of the nanoparticles when in contact with red blood cells, fibroblast cells, and MCF7 cancer cells. Overall, our findings suggest that FN-Ch and FN-CT nanoparticles have potential for use in cancer diagnosis and treatment as part of a new nano-carrier system. Furthermore, combining hyperthermia with other treatment methods could enhance the effectiveness of cancer therapy.

1. Introduction

Hyperthermia (HT) is a least-invasive method for cancer treatment where the target tissues are heated to about 42-46°C. This temperature range is cytotoxic, meaning it is toxic to living cells, specifically tumor cells. Tumor cells have an irregular and compact vascular structure that creates an undesirable microenvironment inside them. This makes them less able to withstand additional heat stress than healthy cells in normal tissue. However, there is a challenge in heating only the local tumor area without damaging the surrounding healthy tissue [1]. To address this challenge, researchers have turned to magnetic nanoparticles (MNs). In recent decades, MNs have become popular in biomedical applications due to their unique properties [2-4]. One promising application of MNs is magnetic liquid hyperthermia (MFH). This is a thermal treatment of cancer cells that is combined with chemotherapy and radiotherapy. MFH uses magnetic nanoparticles as heating agents to overcome the problem of conventional hyperthermia therapy [3]. Magnetic nanoparticles can be remotely controlled and delivered to the target tissues by applying an external magnetic field [5-9]. If these particles are used as drug delivery nanocarriers, a controlled release of the drug can be achieved by creating an alternating magnetic field. Overall, various factors such as the strength of the external magnetic field, magnetic nanoparticles, and hydrodynamic and physiological parameters are effective in treatment with magnetic carriers [10]. Larger particles may also block specific binding sites in cells that inhibit cellular receptors. Nanoparticles have a larger surface-to-volume ratio compared to micro-particles, which means they may offer higher bonding performance [11,12]. The bonding of different parts with nanoparticles expands their application and provides superior properties. Among the various nanoparticles, iron oxide nanoparticles are known as smart drug nanocarriers [13-20]. Iron oxide nanoparticles are a type of magnetic nanoparticle, with Magnetite (Fe_3O_4) and Maghemite (γ-Fe_2O_3) nanoparticles being widely used in biomedical applications. These nanoparticles are small, biocompatible, and can be dispersed in water, making them suitable for use in vivo [4,2]. However, other types of ferrites, obtained by adding ions such as Co^{2+}, Mn^{2+}, and Ni^{2+} to magnetite, have altered magnetic properties and are not as well understood [4].

Ferrites are materials with rich physics and chemistry, with Spinel ferrites, Perovskite ferrites, Garnet ferrites, and hexagonal ferrites being widely studied for their applications in science and technology. Spinel ferrites, for example, are cubic structured materials with tetrahedral and octahedral sublattices that have been studied for their suitability in biomedical, electrical, catalysis, environmental, and other domains [25-27]. The properties and

characteristics of ferrite nanoparticles are affected by their composition and microstructure, which in turn depends on their fabrication method [1]. However, some ferrites have weak magnetic conductivity or toxicity issues that limit their use in biomedical applications. To address these issues, the surface of the particles can be modified with inorganic coatings to improve their magnetic properties or prevent toxicity [23]. Ferrites with the general formula MFe_2O_4, where M = Fe, Mn, Co, have received attention for their magnetic applications due to their easy fabrication, chemical stability, and magnetic tunability [28]. Nickel ferrite ($NiFe_2O_4$) is a suitable candidate for biomedical applications as a substitute for iron oxides (Fe_3O_4 or γ-Fe_2O_3) due to its unique properties such as high bulk saturation magnetization and low magnetic anisotropy [2,3]. These nanoparticles are part of the inverse spinel family and have ferromagnetic properties with high saturation magnetization, mechanical hardness, and excellent chemical stability [29-33]. Nickel ferrite is a potential candidate for medical applications such as MRI contrast agents, drug delivery technology, color imaging, biotechnology, and biomedicine [34-39].

The use of magnetic nanoparticles depends on the fabrication processes used to select optimal conditions and effective methods for their precise design [28]. Several approaches have been developed for the fabrication of $NiFe_2O_4$ nanoparticles, including chemical co-precipitation, Sol-gel method, citrate precursor technique, shock wave technique, mechanical alloying, microwave processing, and aerosolization [2]. In biomedical applications, the leakage of toxic ions from the magnetic core to biological media can be prevented by using suitable surface coatings such as chitosan or CTAB [3]. The introduction of a surface coating also affects the surface anisotropy, which contributes to the magnetic properties of nanoparticles [40]. H. Yin et al. investigated the effect of particle size and surface coating on the cytotoxicity of $NiFe_2O_4$ nanoparticles and found that those encapsulated with Oleic acid displayed no cytotoxic effect [41]. However, despite considerable attention in this field, little research has been done on hyperthermia or MRI applications of surface-coated nickel ferrite nanoparticles, indicating a need for further research. Chitosan and polyethylene glycol (PEG) are the most studied coating materials [3]. S. Bae et al. investigated the hyperthermia properties of $NiFe_2O_4$ particles with different sizes for different applied magnetic fields and frequencies and compared their hyperthermia efficiency with $CoFe_2O_4$ nanoparticles [42]. Lee et al. synthesized spherical nickel ferrite nanoparticles using the thermal decomposition method and investigated the nickel ferrite nanoparticles coated with biocompatible CTAB for use as T2 contrast agents in MRI and heat generators in magnetic hyperthermia [43]. Ahmad et al. synthesized nickel ferrite

($NiFe_2O_4$) nanoparticles coated with cetyltrimethylammonium bromide (CTAB) using a high-temperature thermal decomposition method and investigated their applications in magnetic hyperthermia [44]. Menelaou et al. prepared nickel ferrite nanoparticles coated with cetyltrimethylammonium bromide (CTAB) or 2,3-dimercaptosuccinic acid (DMSA) and reported the values of specific absorption rate (SAR) obtained from hyperthermia experiments at various concentrations in water [45]. S. M. Hoque investigated the effect of induced AC field on heating performance and reported high field NMR relaxation values of different size Chitosan- and PEG-coated $NiFe_2O_4$ nanoparticles [1].

This article presents a comprehensive study on nickel ferrite ($NiFe_2O_4$) nanoparticles coated with Chitosan and Cetyltrimethylammonium Bromide (CTAB). CTAB acts as a biocompatible stabilizer/surfactant and has been used as a coating material in hyperthermia applications with iron oxide nanoparticles. The $NiFe_2O_4$ nanoparticles were synthesized using a new approach, the hydrothermal assisted co-precipitation method, which resulted in no impurity phase in the structure. The structural properties and morphology of the nanoparticles were studied using Thermogravimetric Analysis (TGA), X-Ray Diffraction (XRD), Transmission Electron Microscopy (TEM), Fourier Transform Infrared (FT-IR) spectroscopy, Inductively coupled plasma (ICP), Magnetic Characterization (VSM), and Zeta Potential analyses. To investigate the use of the prepared nanoparticles for cancer treatment with hyperthermia, in vivo studies such as blood hemolysis tests and MTT tests were performed.

2. Materials, Method, and Characterization

2.1. Materials

The primary materials used in the study were $FeCl_3.6H_2O$ and $NiCl_2.6H_2O$ from Merck, Chitosan and CTAB from Sigma, as well as ammonia, ethanol, and deionized water. These materials were used without any purification.

2.2. Methods

2.2.1. Fabrication of Nickel Ferrite ($NiFe_2O_4$) Nanoparticles

The nickel ferrite ($NiFe_2O_4$) nanoparticles were fabricated using the hydrothermal assisted co-precipitation method. A mixture of $FeCl_3.6H_2O$ (2.91 g), $NiCl_2.6H_2O$ (1.26 g) and deionized water (100 ml) was refluxed at 80°C for 15 minutes before adding ammonium hydroxide. The

solution was then kept under reflux for 3 hours at 80°C and placed in a stainless-steel autoclave at 180°C for 8 hours. The resulting precipitate was washed with ethanol and deionized water before being dried in an oven at 50°C for 12 hours. A schematic diagram of the fabrication method is shown in Figure 1.

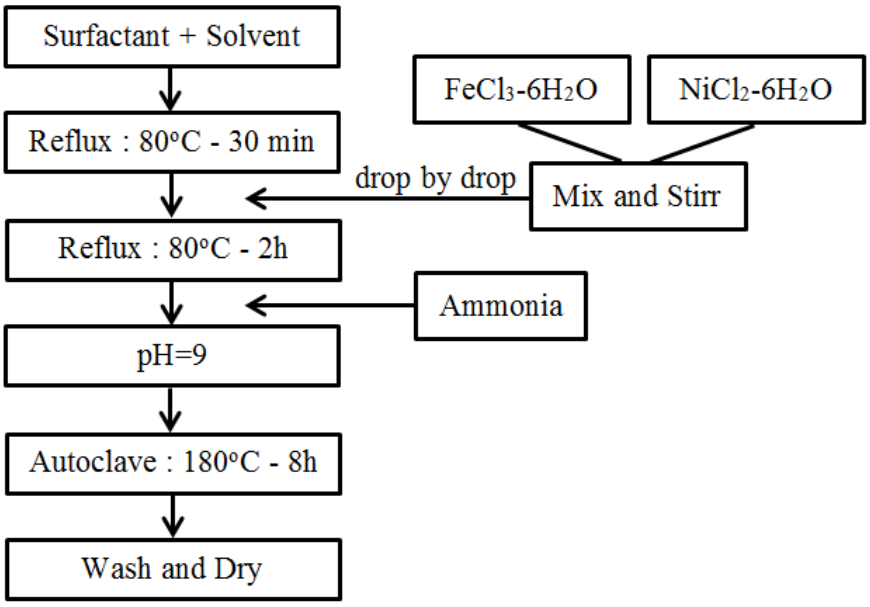

Fig. 1: Schematic diagram of synthesis method of Nickel Ferrite Nanoparticles.

2.2.2. Fabrication of Chitosan-Coated Nickel Ferrite (FN-Ch) Nanoparticles

The FN-Ch nanoparticles were fabricated using the hydrothermal assisted co-precipitation method. A mixture of Chitosan (0.5 g), acetic acid (1 ml), and deionized water (49 ml) was refluxed at 80°C while a separate solution of $FeCl_3.6H_2O$ (2.91 g), $NiCl_2.6H_2O$ (1.26 g), and deionized water (50 ml) was prepared. After 30 minutes of refluxing the Chitosan solution, the Iron and Nickel Chloride solution was added drop by drop and refluxed at 80°C for 2 hours. Ammonia was then added to adjust the pH of the solution to 9 before being refluxed for 3 hours at 80°C. The solution was placed in a stainless-steel autoclave at 180°C for 8 hours. The resulting precipitate was washed with ethanol and deionized water until the pH reached 7 and then dried in an oven at 50°C for 12 hours.

2.2.3. Fabrication of CTAB Coated- Nickel Ferrite (FN-CT) Nanoparticles

CTAB Coated-Nickel Ferrite (FN-CT) nanoparticles were fabricated using a similar method to that of Chitosan-coated-nickel ferrite nanoparticles. The only difference was that CTAB was dissolved in deionized water without adding acetic acid.

2.3. Characterization

The structure of the synthesized nano-powders was examined with an X-ray diffraction (XRD) device, D8 Advance Bruker YT model, and CuKα radiation. Fourier transform infrared spectroscopy, performed with a Nicolet AVATAR 370 model, analyzed the chemical bonds of the samples in the range from 400 to 4000 cm^{-1}. The size and shape of the grains in the nano-powders were studied through transmission electron microscopy (TEM), utilizing an EM 208S model (100KV). Thermal stability in air was evaluated by Thermo gravimetric analysis (TGA) with a Q600 model from TA Company, United States. Zeta potential measurement was conducted with a SZ100 model from Horiba Company, Japan.

3. Results

3.1. Thermo gravimetric Analysis (TGA)

Thermo gravimetric analysis (TGA) was used to evaluate the thermal stability in air of FN, FN-Ch and FN-CT samples. The TGA curves for these samples, shown in Figure 2, indicate weight loss below 200°C due to water absorbed on the surface of both samples. Additionally, significant weight loss between 150 to 300 for FN nanoparticles and 200 to 350°C for both Chitosan- and CTAB-coated samples is mainly due to the loss of low molecular mass compounds, primarily absorbed water. The TGA curve of the coated samples shows a decrease in mass due to decomposition at lower temperatures, consistent with results described elsewhere [46,47].

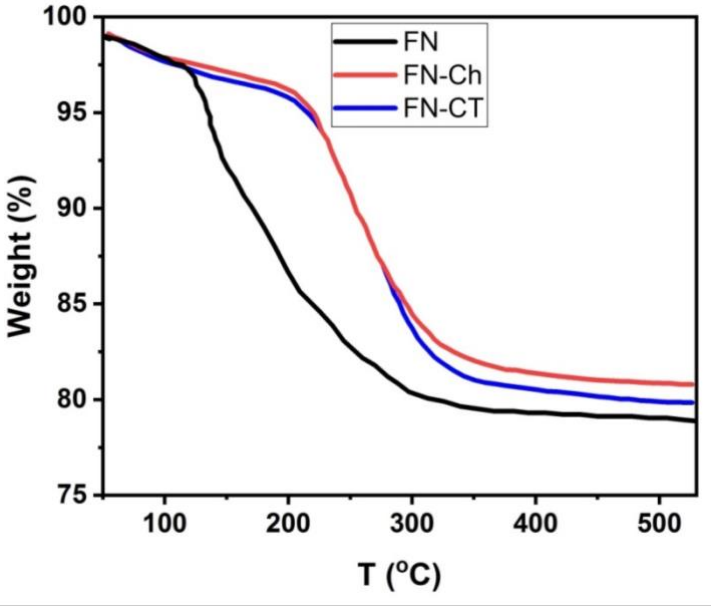

Fig. 2: Thermogravimetric profiles of FN, FN-Ch and FN-CT nanoparticles.

3.2. X-ray Diffraction Analysis

The XRD patterns of FN, FN-Ch and FN-CT nanoparticles are presented in Figure 3. In all three samples, the characteristic diffraction peaks of samples at approximate 2θ values of 18.46°, 30.29°, 35.67°, 37.35°, 43.34°, 53.77°, 57.47°, 63.12°, 71.41°, and 74.69° correspond to the (111), (220), (311), (222), (400), (422), (511), (440), (620) and (533) planes of the spinel structure of $NiFe_2O_4$ (JCPDS card No. 10-0325) [48,49]. The absence of additional peaks for secondary phases indicates that the samples are of high purity. Furthermore, Figure 3 shows that coating nickel ferrite with chitosan and CTAB results in a reduction in the intensity of the peaks, with the reduction being more pronounced in the case of the FN-CT sample. This suggests that the CTAB coating may have a stronger effect on the crystal structure of nickel ferrite nanoparticles compared to the chitosan coating.

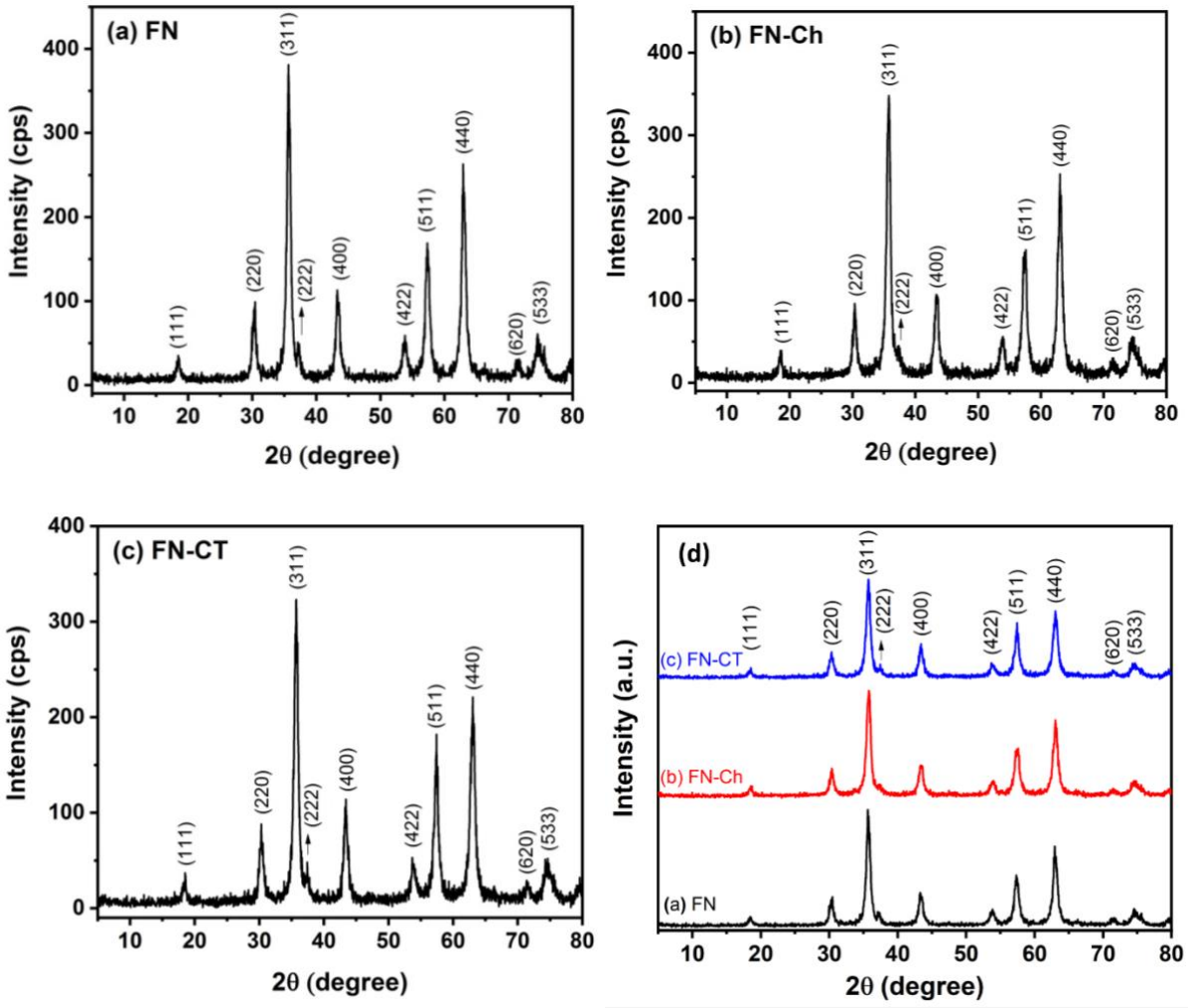

Fig. 3. XRD patterns of (a) FN, (b) FN-Ch, (c) FN-CT nanoparticles and (d) The same patterns in comparison.

Also, Rietveld refinement was carried out for all three samples. The refinements were performed using X'Pert HighScore Plus software, following standard procedures for data preparation, crystal structure modeling, and refinement setup. The results of the Rietveld refinements confirm the purity and phase formation of the samples, with all three samples showing a single-phase spinel structure of Nickel Iron Oxide ($NiFe_2O_4$), as shown in figure 4.

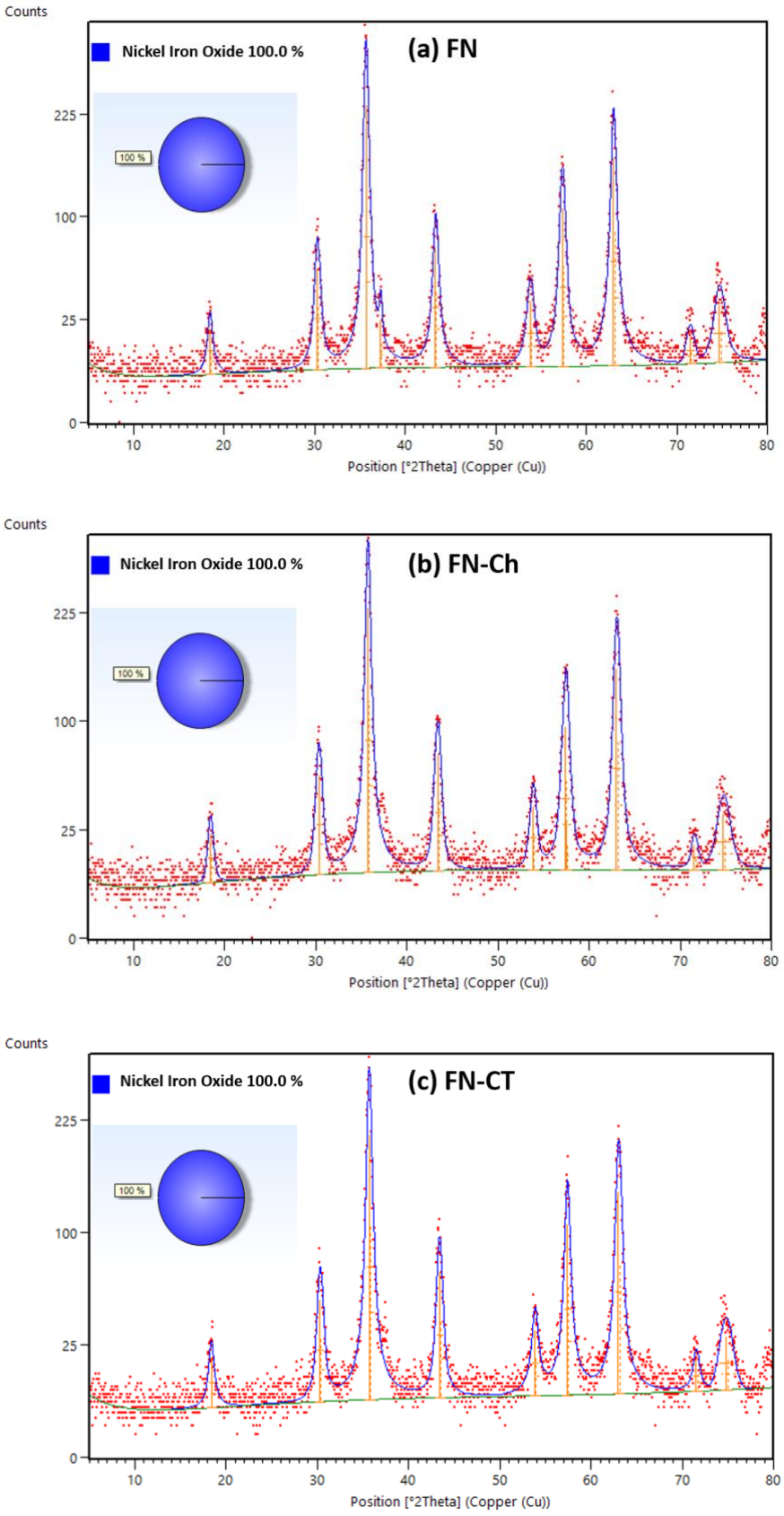

Fig. 4. Refinement results by the Rietveld method using X'Pert HighScore Plus software for (a) FN, (b) FN-Ch and (c) Fn-CT samples.

The crystallite size was calculated for the (311) plane of the pure $NiFe_2O_4$, Chitosan and CTAB coated $NiFe_2O_4$ nanoparticles using the Debye-Scherrer formula, which is as follows:

$$D = \frac{k\lambda}{\beta \cos\theta} \quad (1)$$

Where D is the crystallite size, k is the shape factor, λ is the X-ray wavelength, β is the line broadening at half maximum intensity (FWHM), in radians and θ is the Bragg angle. The XRD parameters are summarized in Table 1. The data provided in Table 1 revealed that the crystallite size has a small decreasing trend with the coating, being approximately 12 nm for all samples [1], indicating that the position and width of the peak significantly is not affected by nickel ferrite coating with chitosan and CTAB.

Table 1. The XRD parameters of FN, FN-Ch and FN-CT nanoparticles

Sample	2θ (°)	d (Å)	β (°)	Intensity (cps)	D (nm)
FN	35.67	2.5152	0.669	381	12.56
FN-Ch	35.71	2.5120	0.672	348	12.54
FN-CT	35.68	2.5143	0.702	323	11.97

3.3. TEM Analysis

TEM was utilized to analyze the shape and size of particles in three samples: FN, FN-Ch, and FN-CT. Figure 5 displays the TEM images of these samples, revealing that all three contain particles with nearly quadrilateral and hexagonal shapes. The coating of nickel ferrite with chitosan and CTAB results in a slight decrease in particle size. However, the FN-Ch sample exhibits more agglomeration of nanoparticles compared to the FN-CT sample. This suggests that the chitosan coating may promote particle agglomeration. In contrast, the particles in both the FN and FN-CT samples are mostly distinct from each other and less agglomerated, indicating that the CTAB coating may inhibit particle agglomeration. The mechanism behind the agglomeration behavior of these two coatings may be different. Chitosan is a biopolymer with a positive charge, which may promote particle agglomeration due to electrostatic

attraction between the particles. CTAB, on the other hand, is a cationic surfactant that can form a bilayer around the nanoparticles, resulting in a stable dispersion and inhibition of particle agglomeration.

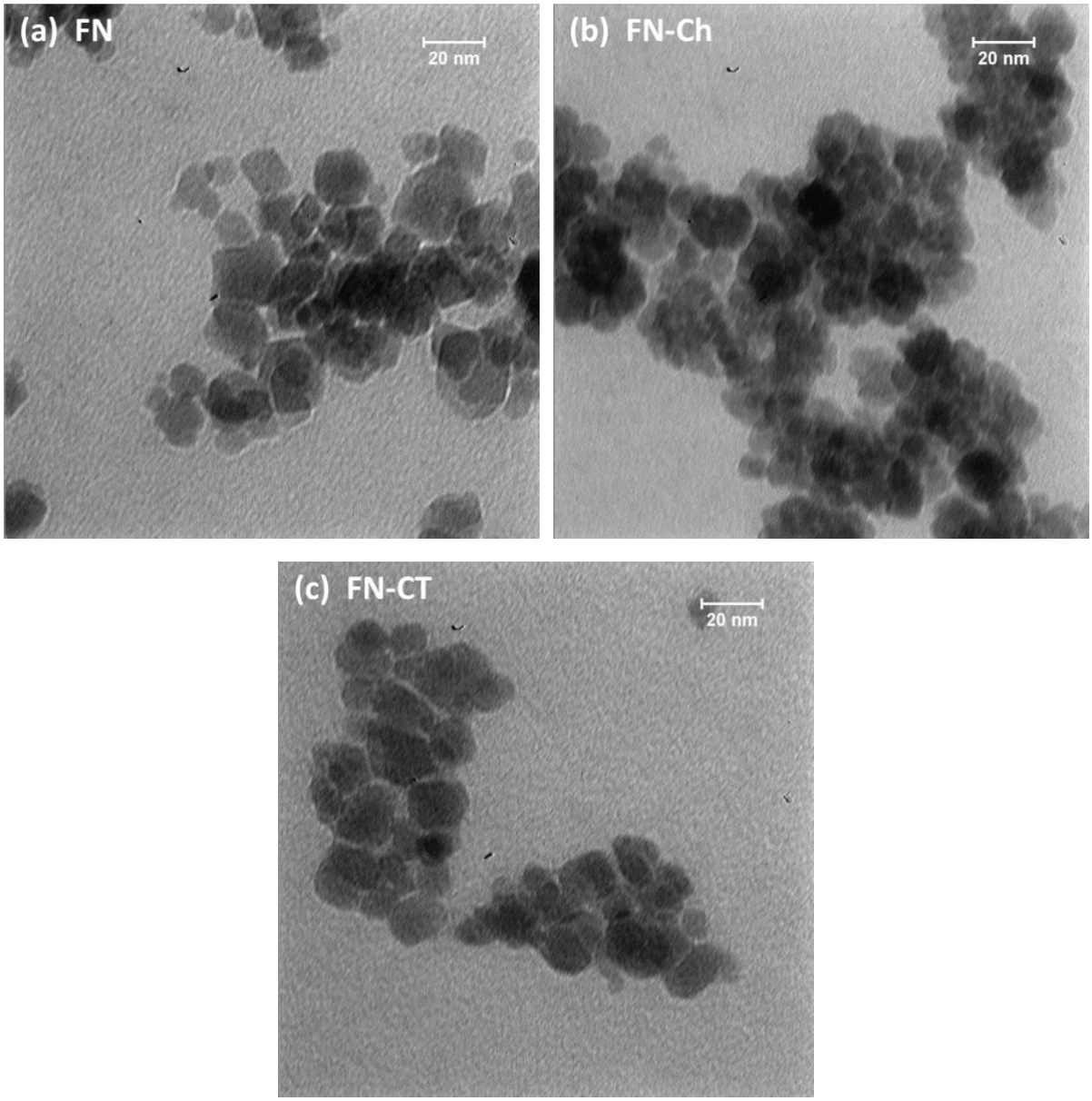

Fig. 5: TEM micrograph of (a) FN (b) FN-Ch and (c) FN-CT nanoparticles.

Image processing software was employed to determine the particle size distribution in all samples using TEM images. As shown in the histogram in Figure 6, there is a trend of decreasing particle size when the samples are coated. The particle sizes for the FN, FN-Ch, and FN-CT samples were found to be within the ranges of 10-12 nm, 10-11 nm, and 9-10 nm, respectively. These results are consistent with those obtained from XRD analysis, which also

indicated that coating FN with chitosan and CTAB resulted in a reduction in particle size compared to the uncoated sample.

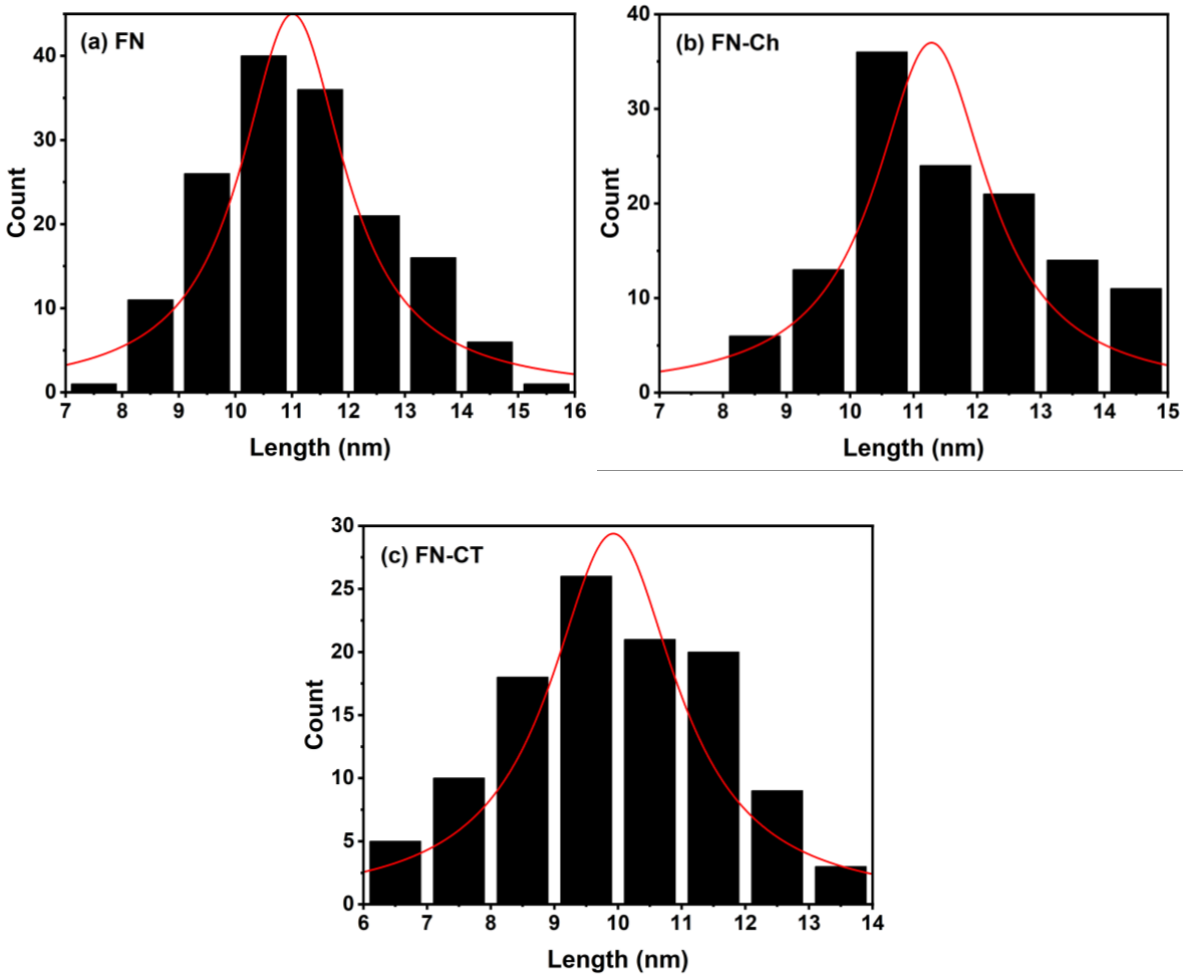

Fig. 6. Particle size distribution from TEM images for (a) FN, (b) FN-Ch and (c) FN-CT nanoparticles.

3.4. Fourier transform infrared (FT-IR) spectroscopy

The presence of Chitosan and CTAB molecules on the surface of synthesized $NiFe_2O_4$ nanoparticles can be confirmed using FT-IR spectroscopy. Figure 7 displays the FTIR spectrum of the prepared samples in the wavelength range of 300-4000 cm^{-1}. The two main metal-oxygen bands, commonly found in the infrared spectrum of all spinel's, particularly ferrites, are also present. The strongest absorption peak (ν_1), typically observed at 604 cm^{-1}, results from stretching vibrations of metal-oxygen bonds in tetrahedral sites within the spinel structure. The lowest band (ν_2), usually observed between 405-601 cm^{-1} (expected around 405 cm^{-1}), is due to metal-oxygen vibrations at octahedral sites [3, 50]. Prominent bands near 3420 and 1650

cm^{-1}, attributed to stretching modes and H-O-H flexural vibrations of free or adsorbed water, are also visible in the spectra. The band near 1400 cm^{-1} results from anti-symmetric NO stretching vibrations caused by nitrate groups remaining in the samples [51]. Figures 7b and 5c present the infrared transmission spectra of coated nanoparticles. The FT-IR spectrum of chitosan-coated nanoparticles (Figure 7b) reveals a shift in absorption lines from ~1158 cm^{-1} to ~897 cm^{-1}. Amide absorption intensifies compared to the pure Chitosan spectrum and shifts to lower wave numbers of ~1645 cm^{-1}, indicative of hydrogen-bonded amides. The sharp peak at ~1376 cm^{-1} results from CH_2 group deformation. Additionally, the tensile bond of OH at 3365 cm^{-1} is associated with OH groups of the hydrogen bond. This suggests a strong hydrogen bond between oxygen in $NiFe_2O_4$ and hydrogen in Chitosan's amino group (NH_2), which also explains the intense absorption of amides in the spectrum of coated particles. These results are consistent with previous observations regarding Chitosan coating on Iron oxide (Fe_3O_4) nanoparticles [52]. Since NH_2 groups are present on both sides of the hydraulic bond used to coat Chitosan, coated particles have a slightly positive charge. As a result, no organic solvent or surfactant is necessary to maintain the colloidal state in the coated particle solution [53]. The coating status of nanoparticles coated with CTAB was also investigated by analyzing their FTIR spectrum, shown in Figure 7c. Peaks at ~408 cm^{-1} correspond to metal-oxygen vibrations (Ni-O and Fe-O). The characteristic band at ~1627cm^{-1} indicates the presence of NH_2 groups on nanoparticle surfaces [54]. The peak at ~1703 cm^{-1} arises from tensile vibrations of CH bonds. The broad peak at 3454 cm^{-1} represents O-H vibrations of hydroxyl groups present in CTAB molecules [45]. All these peaks confirm that nanoparticle surfaces were well covered with CTAB.

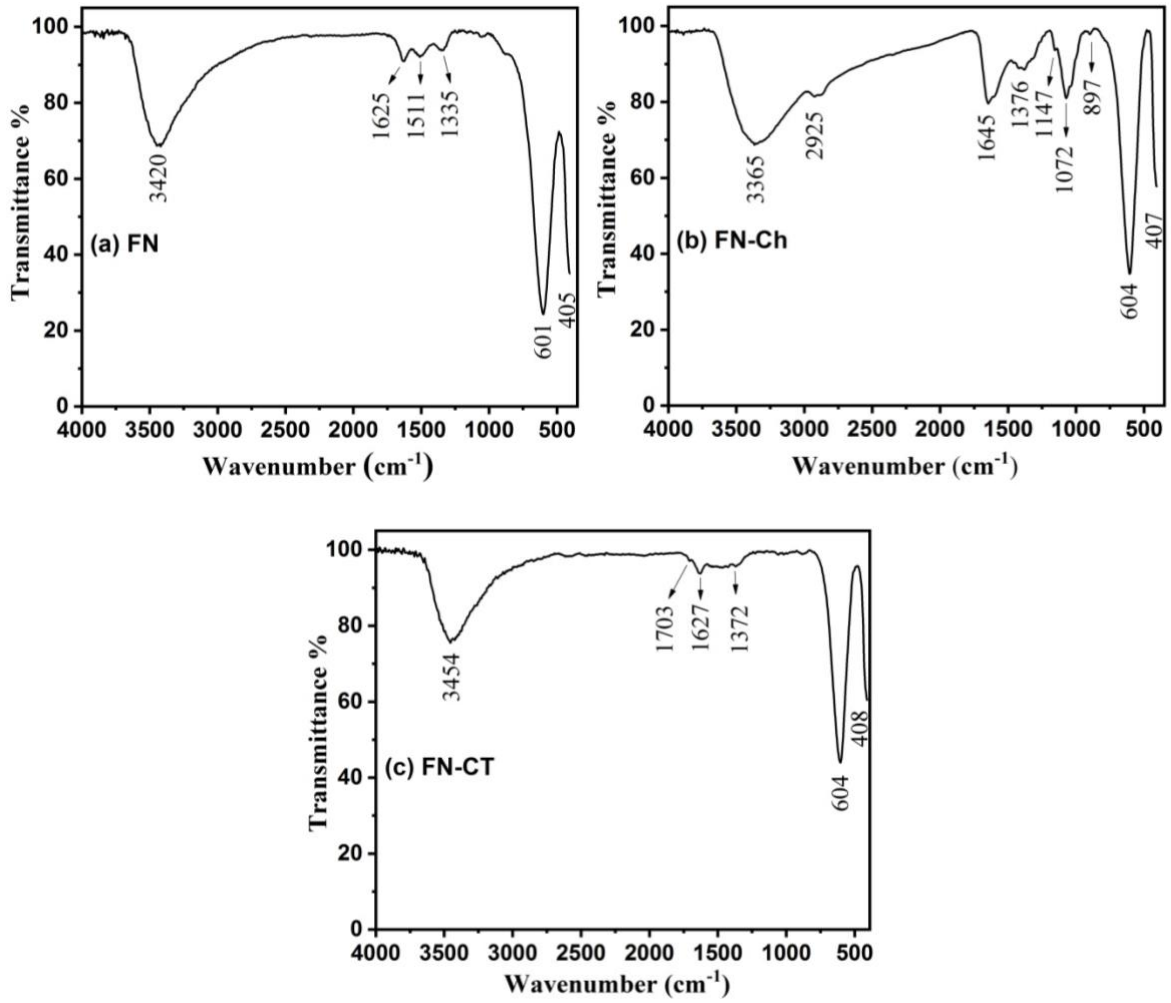

Fig. 7. FTIR spectra of (a) FN, (b) FN-Ch and (c) FN-CT nanoparticles.

3.5. Inductively coupled plasma (ICP) analysis

Inductively coupled plasma (ICP) analysis was performed to determine the elemental composition of the chitosan and CTAB coated nickel ferrite nanoparticles. The results of the ICP analysis provide important information on the elemental composition and purity of the nanoparticles. This information can be useful in determining the suitability of the nanoparticles for biomedical applications, where purity and biocompatibility are critical factors. The samples were prepared by dispersing the nanoparticles in deionized water and subjecting them to ultrasonic treatment for 10 minutes to ensure homogeneity. The concentration of nickel (Ni) and iron (Fe) were determined from the ICP analysis. The analysis was performed in triplicate to ensure the accuracy and reproducibility of the results. The results of the ICP analysis showed that both the chitosan and CTAB coated nickel ferrite nanoparticles were composed of nickel

and iron, as listed in Table 2. No significant amounts of other trace elements were detected in either sample.

Table 2. ICP Analysis Results of FN-Ch and FN-CT Nanoparticles

Sample	Concentration (ppm)	
	Ni	Fe
FN	7.73	14.65
FN-Ch	7.61	14.74
FN-CT	7.67	14.71

3.6. Magnetic Characterization

The magnetic behavior of the synthesized $NiFe_2O_4$ nanoparticles was investigated using a vibrating sample magnetometer (VSM) in the presence of a 20 kOe magnetic field at ambient temperature. Figure 8 shows a magnified view of the M-H curves for the synthesized nanoparticles (nickel ferrite (FN), Chitosan-coated Nickel ferrite (FN-Ch), and CTAB-coated nickel ferrite (FN-CT) nano-powders) in the low-field region to observe the coercivity and remanent magnetization. The inset of Figure 8 shows that the hysteresis loop is shifted from the center, which may be attributed to the presence of magnetic impurities or defects in the nickel ferrite nanoparticles that result in a nonzero net magnetic moment even in the absence of an external magnetic field. According to the hysteresis curve, all synthesized samples exhibit a superparamagnetic structure at room temperature with negligible hysteresis [55-57]. The magnetization value of the nickel ferrite sample decreased in the presence of Chitosan and CTAB surfactants, possibly due to the presence of non-magnetic materials coating the surface of the nickel ferrite [58]. The thicker the coating layer, the greater the reduction in the magnetic properties of the nanoparticles. In addition to the thickness of the coating, factors such as material and particle size also affect the magnetic properties of nanoparticles. The decrease in magnetization was greater in the presence of CTAB than with chitosan.

The values of saturation magnetization (M_s), remanent magnetization (M_r), and coercivity (H_c) were obtained using the hysteresis curve. The saturation magnetization of the synthesized nanoparticle was about M_s=49.7 emu/g at room temperature, lower than the reported value for bulk $NiFe_2O_4$ (M_s=55 emu/g) [3]. This difference may be due to a disordered spin layer at the surface of the nanoparticles that does not contribute to their magnetization [21]. According to

Table 3, all samples have a coercivity of less than 20 Oe, making them suitable for use in hyperthermia applications. In hypothermia applications, magnetic nanoparticles are used to generate heat through magnetic hyperthermia. This is achieved by exposing the nanoparticles to an alternating magnetic field, which causes the magnetic moments of the nanoparticles to rotate and generate heat due to hysteresis losses. The coercivity of magnetic nanoparticles is an important magnetic property that determines their response to an external magnetic field. Nanoparticles with lower coercivity are more easily magnetized and demagnetized by an external magnetic field, which makes them more suitable for magnetic hyperthermia applications. The pure nickel ferrite sample has the lowest coercivity, least magnetic remanence, and highest saturation magnetization. For these samples to be used in hyperthermia applications, H_c must be less than 20 Oe. In both surfactant-coated samples, coercivity is still small enough for use in hyperthermia applications.

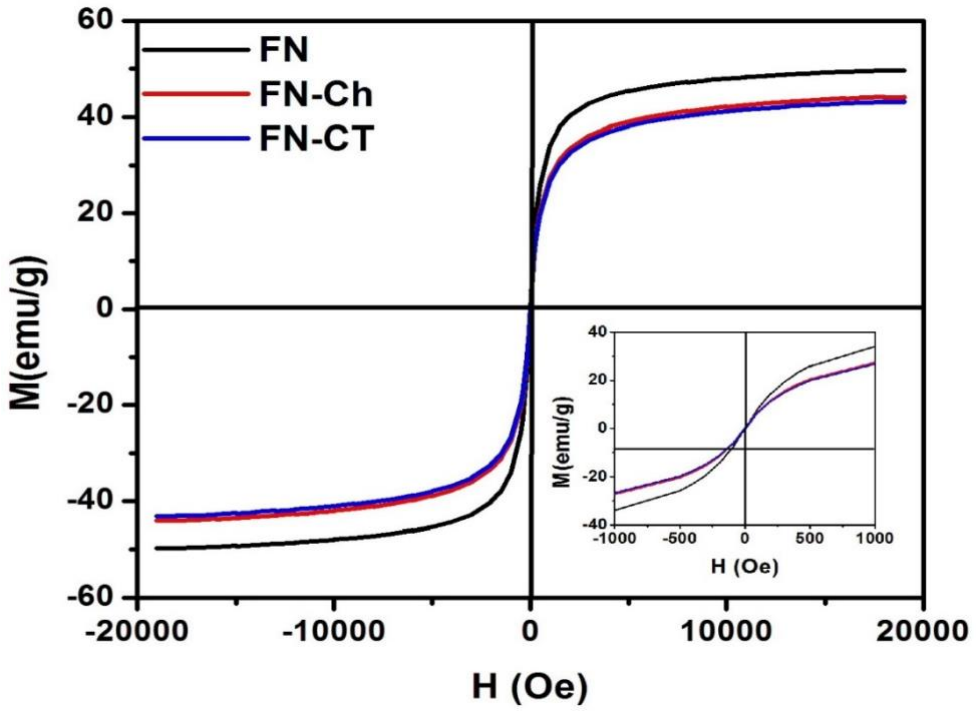

Figure 8: Hysteresis Curve of FN, FN-Ch and FN-CT nanopowders. The inset shows a detail of the hysteresis curve near zero magnetic fields.

Table 3. M_S, M_r and H_c for the FN, FN-Ch and FN-CT nanoparticles.

Samples	M_s (emu/g)	M_r (emu/g)	H_c (Oe)
FN	49.701	0.14168	1.6780

FN-Ch	44.145	0.36461	5.0882
FN-CT	43.172	0.33816	4.9891

3.7. Zeta Potential

The zeta potential test measures the electrical potential difference between the slip layer and the potential at a distance away from the particle. The zeta potential is directly related to the charge density of the particles [59]. The stability of colloids is due to the presence of surface charge on the particles, which causes them to repel each other and prevents them from joining together to form larger lumps [59]. The higher the surface charge of the colloid particles, the more stable the colloid. Figure 9 shows the zeta potential of Chitosan- and CTAB-coated nickel ferrite nanoparticles. The zeta potential for Chitosan- and CTAB-coated nickel ferrite nanoparticles is -32 mV and +25.2 mV, respectively. The absolute value of the zeta potential for both samples is large, indicating good stability [60]. The absolute value of the zeta potential of the chitosan-coated sample is larger, indicating greater stability than with the CTAB surfactant.

The chitosan-coated sample (FN-Ch) had a negative zeta potential, while the CTAB-coated sample (FN-CT) had a positive zeta potential. This difference in zeta potential can be attributed to the differences in the chemical properties of the two coatings. Chitosan is a biopolymer with a positive charge, which may become protonated and neutralized in the acidic environment of the solution, resulting in a negative zeta potential. CTAB, on the other hand, is a cationic surfactant that adsorbs to the particle surface and forms a positively charged bilayer, leading to a positive zeta potential. The difference in zeta potential between the two coatings can affect the shape, morphology, and agglomeration of the prepared nanoparticles. In general, particles with a high zeta potential tend to repel each other and remain dispersed in a solution, while particles with a low zeta potential tend to attract each other and form aggregates or agglomerates. In our study, we observed that the chitosan-coated sample (FN-Ch) exhibited more agglomeration of nanoparticles compared to the CTAB-coated sample (FN-CT), which may be attributed to the negative zeta potential of the chitosan-coated particles. The repulsive forces between the particles are reduced due to the negative zeta potential, resulting in more particle agglomeration. In contrast, the CTAB-coated sample (FN-CT) exhibited less agglomeration, which may be attributed to the positive zeta potential of the CTAB-coated

particles. The repulsive forces between the particles are increased due to the positive zeta potential, resulting in less particle agglomeration.

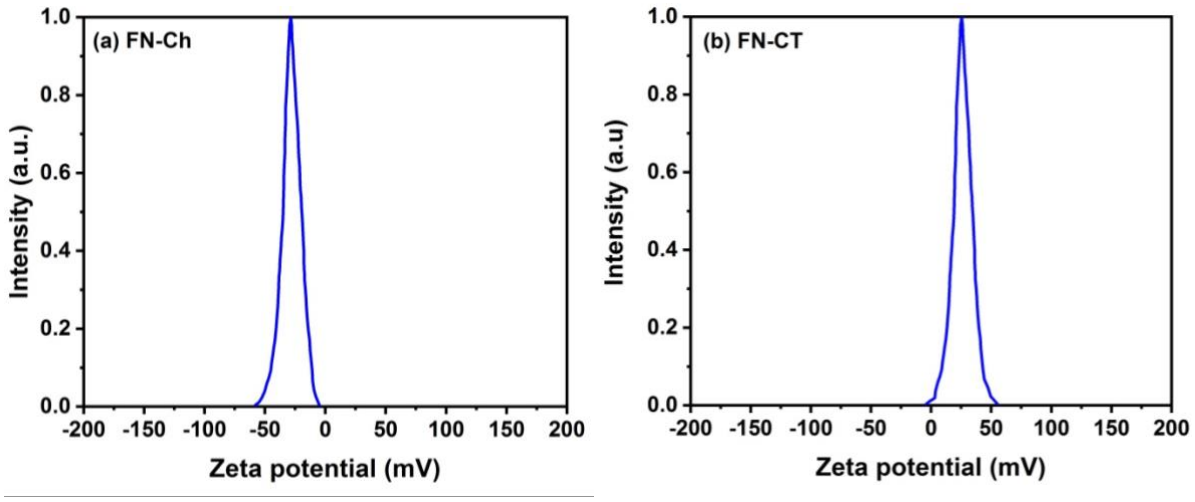

Figure 9: Zeta Potential of (a) FN-Ch and (b) FN-CT nanoparticles.

3.8. Blood Hemolysis Test

A blood hemolysis test was performed to measure the toxicity of nanoparticles in contact with red blood cells. This test evaluates the biocompatibility of nanomaterials by measuring the amount of hemoglobin released and the effect of physical and chemical properties of nanoparticles such as size, porosity, and surface groups on red blood cells [41]. Young human blood was collected in a container containing heparin (4 ml) and centrifuged (2500 rpm for 10 minutes) to separate red blood cells from the serum. The red blood cells were washed and dispersed in RBS (2 ml). Concentrations of 3.125, 6.25, 12.5, 25, 50, and 100 µg/ml were prepared from FN-Ch and FN-CT nanoparticles in RBS. Samples containing 1900 µl of nanoparticles and 100 µl of red blood cells were prepared and incubated in a rotating incubator at 37°C for 24 hours. The samples were then centrifuged and the results were read in a microplate reader at 570 nm. Phosphate Buffer Saline (PBS) solution was used as a negative control that did not cause any blood hemolysis, while 0.1% sodium dodecyl sulfate (SDS) solutions in PBS and distilled water were used as positive controls that caused 100% hemolysis. The results of the blood hemolysis percentage are shown in Figure 10. The hemolysis percentage diagram shows that FN-Ch and FN-CT nanoparticles created approximately the

same amount of red blood cell hemolysis. Both nanoparticles did not show significant hemolysis at low concentrations up to 25 µg/ml, but at concentrations above 50 and 100 µg/ml, their biocompatibility with red blood cells was lower.

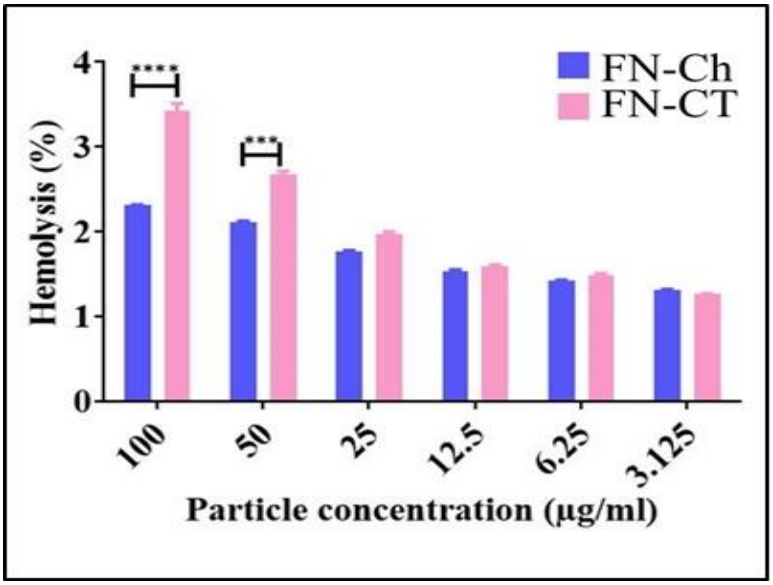

Figure 10: Toxicity Percentage of Blood Hemolysis of FN-Ch and FN-CT Nanoparticles on RBCs.

3.9. MTT Test

The toxicity of the synthesized samples was investigated using the MTT test on Chitosan- and CTAB-coated nickel ferrite nanoparticles in the presence of fibroblast cells (normal cells) and MCF7 cancer cells. To perform the MTT test, 1 mg of each sample was sonicated and dissolved in 100 µl of DMSO solvent at 80°C for 15 minutes before adding 1900 µl of culture medium. DMSO concentration should be 5% of the total volume of the solution since higher percentages are toxic to the cell. The analysis of variance (ANOVA) was performed to compare the groups. The results for fibroblast cells (normal cells) are shown in Figure 11 and Table 4. FN nanoparticles at a concentration of 100 µg/ml were significantly different after 24 and 48 hours. CTAB-coated nanoparticles showed less effect on normal cells at specified concentrations. Both nanoparticles showed the highest percentage of cell killing after 48 hours at low concentrations, with CTAB-coated nickel nanoparticles having a higher effect than Chitosan-coated samples. The results for MCF7 cancer cells are shown in Figure 12 and Table 5. Nickel

ferrite nanoparticles at concentrations of 50 and 500 µg/ml were significantly different after 24 and 48 hours, respectively. Chitosan-coated nanoparticles further reduced the percentage of cell viability at specified concentrations. Both nanoparticles showed the highest percentage of cell killing after 24 and 48 hours at low concentrations (25 and 50 µg/ml), with Chitosan-coated nickel nanoparticles having a more significant effect, especially at a concentration of 50 µg/ml, than CTAB samples. IC50 is a concentration of drugs that stops cell growth by 50% compared to controls [61,62]. Based on the results obtained, FN-Ch nanoparticles can have a good anti-cancer effect, but further biological evaluations are needed. Figure 13 shows that the viability of chitosan-bounded Nickel ferrite nanoparticles in MCF7 and NIH cells at concentrations of 25, 75, and 100 is significantly different. This compound is more toxic to MCF7 cancer cells and less toxic to normal fibroblast cells. The mechanistic pathways for the roles of the Chitosan coated nickel ferrite and CTAB coated nickel ferrite nanoparticles against cancer cells may involve multiple processes. One potential mechanism is the generation of reactive oxygen species (ROS) by the nanoparticles. ROS are known to play a crucial role in inducing apoptosis (programmed cell death) in cancer cells. It is possible that the Chitosan and CTAB coatings on the nICanoparticles may help to enhance ROS generation by the nanoparticles, leading to increased apoptosis in cancer cells. Another possible mechanism is the inhibition of cell proliferation and growth by the nanoparticles. The Chitosan and CTAB coatings may help to increase the cellular uptake of the nanoparticles, leading to increased accumulation of the nanoparticles within the cancer cells. This accumulation may disrupt cellular processes, leading to the inhibition of cell proliferation and growth. Additionally, it is possible that the magnetic properties of the nickel ferrite nanoparticles may play a role in their anti-cancer effects. The nanoparticles may be able to induce hyperthermia (localized heating) within the cancer cells when exposed to an alternating magnetic field, leading to apoptosis and cell death. Finally, the Chitosan and CTAB coatings on the nanoparticles may help to increase their stability and biocompatibility, making them better suited for use in biomedical applications. This may allow for more effective and targeted delivery of the nanoparticles to cancer cells, increasing their anti-cancer effects. In summary, the proposed mechanistic pathways for the roles of the Chitosan coated nickel ferrite and CTAB coated nickel ferrite nanoparticles against cancer cells may involve multiple mechanisms, including ROS generation, inhibition of cell proliferation and growth, hyperthermia induction, and increased stability and biocompatibility.

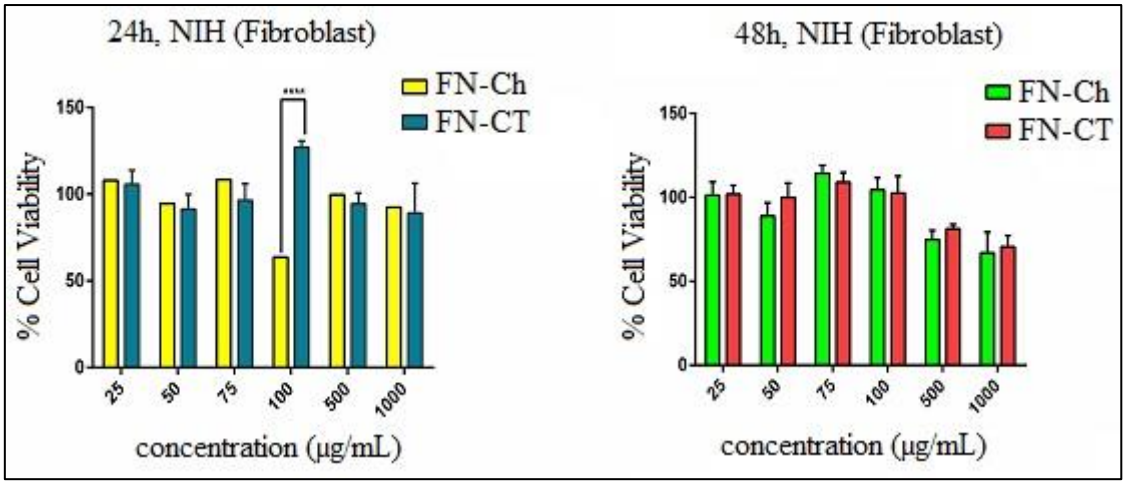

Figure 11: MTT assay. Cell viability of FN-Ch and FN-CT in NIH (Fibroblast) cells exposed to various concentrations after 24h and 48h (n=4). * indicates a significant difference between the two types of Nanoparticles (NPs). *P* values was defined as *$P \leq 0.05$, ** $P \leq 0.01$, *** $P \leq 0.001$ and **** $P \leq 0.0001$.

Table 4. Cytotoxic activity ($IC_{50,}$ µM) of FN-Ch and FN-CT against NIH (Fibroblast) Normal cell line.

Treatment	Sample	
	FN-Ch	FN-CT
IC_{50} (µg/ml), 24h	81.68±0.29	213.70±0.67
IC_{50} (µg/ml), 48h	168.5±0.13	248.40±0.09

Table 5. Cytotoxic activity (IC_{50}) of FN-Ch and FN-CT against MCF7 cancer cell line.

Treatment	Sample	
	FN-Ch	FN-CT
IC_{50} (µg/ml), 24h	21.15±0.12	51.90±0.07
IC_{50} (µg/ml), 48h	18.42±0.14	28.40±0.22

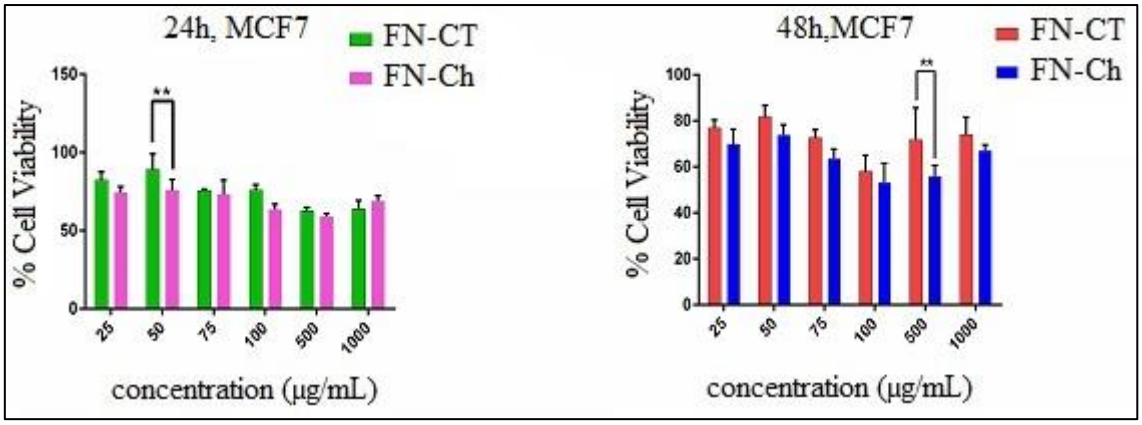

Figure 12: MTT assay. Cell viability of FN-Ch and FN-CT in MCF7 cells exposed to various concentrations after 24h and 48h (n=4). * Indicates a significant difference between two types of Nanoparticles (NPs). *P* values was defined as *$P \leq 0.05$, ** $P \leq 0.01$, *** $P \leq 0.001$ and **** $P \leq 0.0001$.

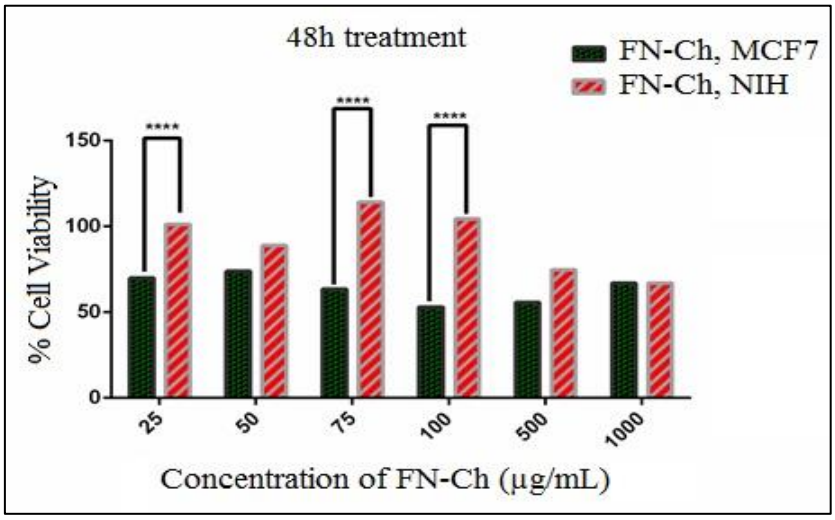

Figure 13: MTT assay. Cell viability of FN-Ch in MCF7 and NIH (Fibroblast) cells exposed to various concentrations after 48h (n=4). * Indicates a significant difference between two types of Nanoparticles (NPs). *P* values was defined as *$P \leq 0.05$, ** $P \leq 0.01$, *** $P \leq 0.001$ and **** $P \leq 0.0001$.

4. Conclusion

In conclusion, this study investigated the hyperthermia characteristics of nickel ferrite ($NiFe_2O_4$) nanoparticles synthesized using a hydrothermal assisted co-precipitation approach and coated with Chitosan and cetyltrimethylammonium bromide (CTAB) to hinder the possible toxic effect of Nickel. Thermal stability in air was evaluated for nickel ferrite, Chitosan coated nickel ferrite and CTAB coated nickel ferrite using calorimetric analysis, which showed weight loss due to water absorbed on the surface of the samples. XRD results confirmed the formation of nickel ferrite without any impurities. TEM images showed uniform particle size distribution with grain size in the shape of nearly quadrilateral and hexagonal. FT-IR analysis detected chemical groups related to the presence of Chitosan and CTAB molecules on the surface of nanoparticles. The magnetic properties of the synthesized nanopowders were investigated using a vibrating sample magnetometer (VSM) in the presence of a 20 kOe magnetic field at room temperature. The hysteresis curve showed superparamagnetic behavior at room temperature with negligible hysteresis for all as-prepared nanoparticles. However, the magnetization value of the nickel ferrite nanoparticle decreased in the presence of Chitosan and CTAB surfactants. The blood hemolysis test was performed to measure the toxicity of nanoparticles in contact with red blood cells. Both FN-Ch and FN-CT nanoparticles showed no significant hemolysis at low concentrations up to 25 µg/ml, but at concentrations above 50 and 100 µg/ml, their biocompatibility with red blood cells was lower. The MTT test was performed on Chitosan- and CTAB-coated nickel ferrite nano-powder in the presence of fibroblast cells (normal cells) and MCF7 cancer cells. FN nanoparticles at a concentration of 100 µg/ml were significantly different after 24 and 48 hours, while CTAB-coated nanoparticles showed less effect on normal cells. Overall, this research fabricated and characterized chitosan-CTAB@$NiFe_2O_4$ nanoparticles for use in hyperthermia treatment and performed in vivo studies (Blood Hemolysis Test and MTT Test) on the synthesized nanoparticles. The findings show that Chitosan/CTAB-coated Nickel ferrite (Ch-CTAB@$NiFe_2O_4$) nanoparticles at low concentrations are suitable for applications as heat generators in magnetic hyperthermia.

5. References:

1. Hoque, S.M., et al., *Thermo-therapeutic applications of chitosan-and PEG-coated $NiFe_2O_4$ nanoparticles.* Nanotechnology, 2016. **27**(28): p. 285702.
2. Yang, H., et al., *Formation of $NiFe_2O_4$ nanoparticles by mechanochemical reaction.* Materials Research Bulletin, 2004. **39**(6): p. 833-837.
3. Umut, E., et al., *Nickel ferrite nanoparticles for simultaneous use in magnetic resonance imaging and magnetic fluid hyperthermia.* Journal of colloid and interface science, 2019. **550**: p. 199-209.
4. ÇE, D.D., et al., *Comparative Heating Efficiency of Cobalt-, Manganese-, and Nickel-Ferrite Nanoparticles for a Hyperthermia Agent in Biomedicines.* ACS Applied Materials & Interfaces, 2019. **11**(7): p. 6858-6866.
5. Moghanizadeh, A., et al., *RETRACTED ARTICLE: Study the effect of static magnetic field intensity on drug delivery by magnetic nanoparticles.* Scientific Reports, 2021. **11**(1): p. 18056.
6. Patra, J.K., et al., *Nano based drug delivery systems: recent developments and future prospects.* Journal of nanobiotechnology, 2018. **16**(1): p. 1-33.
7. Mody, V.V., A. Singh, and B. Wesley, *Basics of magnetic nanoparticles for their application in the field of magnetic fluid hyperthermia.* European Journal of Nanomedicine, 2013. **5**(1): p. 11-21.
8. Ali, A., et al., *Review on recent progress in magnetic nanoparticles: Synthesis, characterization, and diverse applications.* Frontiers in chemistry, 2021. **9**: p. 629054.
9. Sensenig, R., et al., *Magnetic nanoparticle-based approaches to locally target therapy and enhance tissue regeneration in vivo.* Nanomedicine, 2012. **7**(9): p. 1425-1442.
10. Reddy, M.P. and A. Mohamed, *One-pot solvothermal synthesis and performance of mesoporous magnetic ferrite MFe_2O_4 nanospheres.* Microporous and Mesoporous Materials, 2015. **215**: p. 37-45.
11. Chenthamara, D., et al., *Therapeutic efficacy of nanoparticles and routes of administration.* Biomaterials research, 2019. **23**(1): p. 1-29.
12. Ashraf, M.A., et al., *Effects of size and aggregation/agglomeration of nanoparticles on the interfacial/interphase properties and tensile strength of polymer nanocomposites.* Nanoscale research letters, 2018. **13**: p. 1-7.
13. Meng, Q., et al., *Review on design strategies and considerations of polysaccharide-based smart drug delivery systems for cancer therapy.* Carbohydrate Polymers, 2021: p. 119013.
14. Phogat, S., et al., *Diatom mediated smart drug delivery system.* Journal of Drug Delivery Science and Technology, 2021. **63**: p. 102433.
15. Zhang, H., et al., *Recent advances of two-dimensional materials in smart drug delivery nano-systems.* Bioactive Materials, 2020. **5**(4): p. 1071-1086.
16. Shi, Z., et al., *Inorganic nano-carriers based smart drug delivery systems for tumor therapy.* Smart Materials in Medicine, 2020. **1**: p. 32-47.
17. Mabrouk, M., et al., *Hepatotoxic and neurotoxic potential of iron oxide nanoparticles in wistar rats: a biochemical and ultrastructural study.* Biological Trace Element Research, 2021: p. 1-28.
18. Ghitman, J., et al., *Review of hybrid PLGA nanoparticles: Future of smart drug delivery and theranostics medicine.* Materials & Design, 2020. **193**: p. 108805.
19. Aisida, S.O., et al., *Bio-inspired encapsulation and functionalization of iron oxide nanoparticles for biomedical applications.* European polymer journal, 2020. **122**: p. 109371.

20. Hashemzadeh, A., et al., *When metal–organic framework mediated smart drug delivery meets gastrointestinal cancers.* Journal of Materials Chemistry B, 2021. **9**(19): p. 3967-3982.
21. Kodama, R.H., et al., *Surface spin disorder in $NiFe_2O_4$ nanoparticles.* Physical Review Letters, 1996. **77**(2): p. 394.
22. Kang, D., et al., *One-step fabrication and characterization of hierarchical $MgFe_2O_4$ microspheres and their application for lead removal.* Microporous and Mesoporous Materials, 2015. **207**: p. 170-178.
23. Varadavenkatesan, T., et al., *Synthesis, biological and environmental applications of hydroxyapatite and its composites with organic and inorganic coatings.* Progress in Organic Coatings, 2021. **151**: p. 106056.
24. Ramana, P., et al., *A study of uncoated and coated nickel-zinc ferrite nanoparticles for magnetic hyperthermia.* Materials Chemistry and Physics, 2021. **266**: p. 124546.
25. Vickers, N.J., *Animal communication: when i'm calling you, will you answer too?* Current biology, 2017. **27**(14): p. R713-R715.
26. Das, K.C. and S.S. Dhar, *Rapid catalytic degradation of malachite green by MgFe2O4 nanoparticles in presence of H_2O_2.* Journal of Alloys and Compounds, 2020. **828**: p. 154462.
27. Xiao, Y. and J. Du, *Superparamagnetic nanoparticles for biomedical applications.* Journal of Materials Chemistry B, 2020. **8**(3): p. 354-367.
28. Makridis, A., et al., *A facile microwave synthetic route for ferrite nanoparticles with direct impact in magnetic particle hyperthermia.* Materials Science and Engineering: C, 2016. **63**: p. 663-670.
29. Madhalea, K.V., M. Salunkhe, and S. Bangale, *Structural, morphological and hydrophilic properties of nanocrystalline $NiFe_2O_4$ by combustion route.* Archives of Applied Science Research, 2013. **5**(1): p. 62-67.
30. Perron, H., et al., *Structural investigation and electronic properties of the nickel ferrite $NiFe_2O_4$: a periodic density functional theory approach.* Journal of Physics: Condensed Matter, 2007. **19**(34): p. 346219.
31. Ueno, T., et al., *Practical and potential applications of soft magnetic powder cores with superior magnetic properties.* SEI Technical Review, 2016(82): p. 9.
32. Anirudhan, T., V. Manjusha, and F. Shainy, *Magnetically retrievable cysteine modified graphene oxide@ nickelferrite@ titanium dioxide photocatalyst for the effective degradation of chlorpyrifos from aqueous solutions.* Environmental Technology & Innovation, 2021. **23**: p. 101633.
33. Sohail, M., et al., *Synthesis of well-dispersed TiO_2/CNTs@ $CoFe_2O_4$ nanocomposites and their photocatalytic properties.* Materials Research Bulletin, 2018. **101**: p. 83-89.
34. Baig, M.M., E. Pervaiz, and M.J. Afzal, *Catalytic activity and kinetic studies of Core@ Shell nanostructure $NiFe_2O_4$@ TiO_2 for photocatalytic degradation of methyl orange dye.* J. Chem. Soc. Pak, 2020. **42**(04): p. 531.
35. Hossain, M.K., M.I. Khan, and A. El-Denglawey, *A review on biomedical applications, prospects, and challenges of rare earth oxides.* Applied Materials Today, 2021. **24**: p. 101104.
36. Nasiri, R., N. Arsalani, and Y. Panahian, *One-pot synthesis of novel magnetic three-dimensional graphene/chitosan/nickel ferrite nanocomposite for lead ions removal from aqueous solution: RSM modelling design.* Journal of Cleaner Production, 2018. **201**: p. 507-515.
37. Rabiee, N., et al., *Diatoms with invaluable applications in nanotechnology, biotechnology, and biomedicine: recent advances.* ACS biomaterials science & engineering, 2021. **7**(7): p. 3053-3068.

38. Javed, R., et al., *Role of capping agents in the application of nanoparticles in biomedicine and environmental remediation: recent trends and future prospects.* Journal of Nanobiotechnology, 2020. **18**: p. 1-15.
39. Sriplai, N. and S. Pinitsoontorn, *Bacterial cellulose-based magnetic nanocomposites: A review.* Carbohydrate Polymers, 2021. **254**: p. 117228.
40. Raland, R. and J. Borah, *Efficacy of heat generation in CTAB coated Mn doped ZnFe2O4 nanoparticles for magnetic hyperthermia.* Journal of Physics D: Applied Physics, 2016. **50**(3): p. 035001.
41. Yin, H., H. Too, and G. Chow, *The effects of particle size and surface coating on the cytotoxicity of nickel ferrite.* Biomaterials, 2005. **26**(29): p. 5818-5826.
42. Bae, S., et al., *AC magnetic-field-induced heating and physical properties of ferrite nanoparticles for a hyperthermia agent in medicine.* IEEE Transactions on nanotechnology, 2008. **8**(1): p. 86-94.
43. Lee, D.-A., H. Bae, and I. Rhee, *Cetyl Trimethyl Ammonium Bromide-coated Nickel Ferrite Nanoparticles for Magnetic Hyperthermia and T 2 Contrast Agents in Magnetic Resonance Imaging.* Journal of the Korean Physical Society, 2018. **73**: p. 1334-1339.
44. Ahmad, A., H. Bae, and I. Rhee, *Cube-Shaped Cetyltrimethyl Ammonium Bromide-Coated Nickel Ferrite Nanoparticles for Hyperthermia Applications.* Journal of the Korean Physical Society, 2018. **73**: p. 125-129.
45. Menelaou, M., et al., *Evaluation of nickel ferrite nanoparticles coated with oleylamine by NMR relaxation measurements and magnetic hyperthermia.* Dalton Transactions, 2014. **43**(9): p. 3626-3636.
46. Shete, P., et al., *Magnetic chitosan nanocomposite for hyperthermia therapy application: Preparation, characterization and in vitro experiments.* Applied Surface Science, 2014. **288**: p. 149-157.
47. Qu, J., et al., *Preparation of Fe3O4–chitosan nanoparticles used for hyperthermia.* Advanced Powder Technology, 2010. **21**(4): p. 461-467.
48. Younas, M., et al., *Metal-semiconductor transition in $NiFe_2O_4$ nanoparticles due to reverse cationic distribution by impedance spectroscopy.* Journal of Applied Physics, 2011. **109**(9): p. 093704.
49. Amar, V., J. Puszynski, and R. Shende, *H_2 generation from thermochemical water-splitting using yttria stabilized $NiFe_2O_4$ core-shell nanoparticles.* Journal of Renewable and Sustainable Energy, 2015. **7**(2): p. 023113.
50. Waldron, R., *Infrared spectra of ferrites.* Physical review, 1955. **99**(6): p. 1727.
51. Priyadharsini, P., et al., *Structural, spectroscopic and magnetic study of nanocrystalline Ni–Zn ferrites.* Materials Chemistry and Physics, 2009. **116**(1): p. 207-213.
52. Hong, S., Y. Chang, and I. Rhee, *Chitosan-coated ferrite (Fe_3O_4) nanoparticles as a T2 contrast agent for magnetic resonance imaging.* J. Korean Phys. Soc, 2010. **56**(3): p. 868-873.
53. Tan, W.B. and Y. Zhang, *Surface modification of gold and quantum dot nanoparticles with chitosan for bioapplications.* Journal of Biomedical Materials Research Part A: An Official Journal of The Society for Biomaterials, The Japanese Society for Biomaterials, and The Australian Society for Biomaterials and the Korean Society for Biomaterials, 2005. **75**(1): p. 56-62.
54. Zhang, H.-F. and Y.-P. Shi, *Pretreatment properties of CTAB coated Fe3O4 nanoparticle mixed hemimicelle sorbents for the analysis of herbal medicine samples.* Current Analytical Chemistry, 2012. **8**(1): p. 150-158.
55. Kurmude, D., et al., *Superparamagnetic behavior of zinc-substituted nickel ferrite nanoparticles and its effect on mossbauer and magnetic parameters.* Journal of Superconductivity and Novel Magnetism, 2014. **27**: p. 1889-1897.

56. Deb, P., A. Basumallick, and S. Das, *Controlled synthesis of monodispersed superparamagnetic nickel ferrite nanoparticles.* Solid state communications, 2007. **142**(12): p. 702-705.
57. Nogueira, N.A.d.S., et al., *X-ray diffraction and Mossbauer studies on superparamagnetic nickel ferrite ($NiFe_2O_4$) obtained by the proteic sol–gel method.* Materials Chemistry and Physics, 2015. **163**: p. 402-406.
58. Reddy, D.H.K. and Y.-S. Yun, *Spinel ferrite magnetic adsorbents: alternative future materials for water purification?* Coordination Chemistry Reviews, 2016. **315**: p. 90-111.
59. Bhosale, S., et al., *Effect of surface properties of $NiFe_2O_4$ nanoparticles synthesized by dc thermal plasma route on antimicrobial activity.* Applied Surface Science, 2018. **441**: p. 724-733.
60. Bhosale, S.V., et al., *Micro-structural analysis of NiFe 2 O 4 nanoparticles synthesized by thermal plasma route and its suitability for BSA adsorption.* Journal of Materials Science: Materials in Medicine, 2015. **26**: p. 1-15.
61. Mushtaq, S., et al., *Biocompatibility and cytotoxicity in vitro of surface-functionalized drug-loaded spinel ferrite nanoparticles.* Beilstein Journal of Nanotechnology, 2021. **12**(1): p. 1339-1364.
62. Ranji-Burachaloo, H., et al., *Cancer treatment through nanoparticle-facilitated fenton reaction.* Acs Nano, 2018. **12**(12): p. 11819-11837.